NASA TN D-688

TECHNICAL NOTE

D-688

SURFACE PRESSURES AND HEAT TRANSFER ON UNSWEPT BLUNT PLATES IN HELIUM AT HIGH MACH NUMBERS

By Joseph G. Marvin

Ames Research Center
Moffett Field, Calif.

NATIONAL AERONAUTICS AND SPACE ADMINISTRATION
WASHINGTON

March 1961

NATIONAL AERONAUTICS AND SPACE ADMINISTRATION

TECHNICAL NOTE D-688

SURFACE PRESSURES AND HEAT TRANSFER ON UNSWEPT BLUNT PLATES IN HELIUM AT HIGH MACH NUMBERS

By Joseph G. Marvin

SUMMARY

Pressure distributions and local convective heat-transfer coefficients on a flat plate at zero angle of attack were measured in helium. Data were obtained with various amounts of leading-edge bluntness at Mach numbers of 12.5 and 14.7. The pressures on a sharp leading-edged plate were not influenced by the leading edge and were predicted by the first-order, hypersonic, weak-interaction theory. Pressures on blunt plates were correlated by introducing the leading-edge Reynolds number as a parameter. Measured heat-transfer coefficients on the sharp plate agreed with predictions obtained from existing exact solutions for heat transfer across the laminar boundary layer. For the blunt plates a comparison of theory with experiment indicated that more knowledge of the flow field between the shock wave and plate surface is necessary before an adequate prediction of convective heat transfer can be made.

Shock-wave shapes for the blunt plates at a Mach number 12.5 and zero angle of attack were measured. At distances between 2 and 60 leading-edge thicknesses from the shock vertex, the shock-wave shapes were found to be represented by a modified form of the blast-wave analogy.

INTRODUCTION

Investigators have had considerable success in correlating skin-friction measurements obtained in helium at supersonic speeds with those obtained in air at similar test conditions (see ref. 1). Correlations have also been made between measurements in helium and air of the induced pressure rise on flat plates at supersonic speeds (e.g., ref. 2). Much of the testing in helium at very high Mach numbers has been undertaken to evaluate methods for predicting surface pressures on simple aerodynamic shapes (see refs. 3 and 4). In light of the results of reference 1 and insofar as Reynolds analogy is applicable, helium can be used in similar investigations of heat transfer to such shapes.

The purpose of the present tests was: (1) to examine the pressure distribution on flat plates over a range of leading-edge Reynolds numbers from 600 to 120,000, and (2) to compare measured heat-transfer coefficients with values obtained from theory to determine if available theories were adequate for predicting heat-transfer rates in a high-speed gas flow where the complicating factors associated with air chemistry were present.

SYMBOLS

C	thermal capacity per square foot of heat-transfer area, Btu/ft^2, $^\circ$F
C_{D_N}	nose drag coefficient, dimensionless
c_p	specific heat at constant pressure, Btu/lb, $^\circ$F
C_w	constant in linear viscosity relation
d	leading-edge diameter, in.
h	local convective heat-transfer coefficient, Btu/hr, ft^2, $^\circ$F
i	enthalpy, Btu/lb
k	thermal conductivity, Btu/hr, ft^2, $^\circ$F, ft
K	constant of proportionality in equation (5)
K_1	constant of proportionality in equation (4)
l	distance along nozzle center line measured from the nozzle throat, in.
M	Mach number, dimensionless
n	exponent for the sharp-plate pressure variation with x, $(p \sim x^n)$
p	surface pressure, lb/sq ft
p_∞	free-stream static pressure in empty tunnel, lb/sq ft
Δp	pressure increment above free-stream static pressure $(p-p_\infty)$, lb/sq ft
Pr	Prandtl number, $\frac{c_p \mu}{k}$, dimensionless

R perpendicular distance to the outer edge of the shock wave from a plane parallel to the free stream and passing through the vertex of the shock wave, in.

Re_d Reynolds number based on leading-edge diameter, $\frac{\rho_\infty u_\infty d}{\mu_\infty}$, dimensionless

Re_s Reynolds number based on length of boundary-layer run, $\frac{\rho u s}{\mu}$, dimensionless

s distance along the body surface measured from the stagnation point, ft

S_w enthalpy function $\left(\frac{i_w}{i_t} - 1\right)$, dimensionless

T temperature, $^\circ R$

t thickness of leading edge, in.

u velocity, ft/sec

x perpendicular distance from a plane tangent to the nose and perpendicular to the plate surface, in.

x_o distance from foremost point of detached shock to intercept of its asymptote on the x axis, in.

β_o cotangent of the asymptote of the hyperbola in equation (6)

γ ratio of specific heats

δ oblique shock-wave angle measured from upstream flow direction

η inclination angle of boundary layer to the free-stream direction

θ time, hr

μ viscosity, lb/sec ft

χ_∞ hypersonic viscous interaction parameter, $\frac{M_\infty^3 \sqrt{C_w}}{\sqrt{Re_{s_\infty}}}$

ρ density, lb/cu ft

Δ detachment distance of the shock wave, in.

Subscripts

e	edge of the boundary layer
r	recovery value
t	free-stream stagnation value
w	wall or surface value
∞	undisturbed free-stream conditions

Superscripts

*	evaluation of fluid properties at the reference temperature defined by the equation $\frac{T^*}{T_e} = 1 + 0.032Me^2 + 0.58\left(\frac{T_w}{T_e} - 1\right)$
'	differentiation with respect to a transformed variable

APPARATUS

Tunnel

The tests were made in the helium pilot tunnel shown in figure 1. Helium was supplied at 2400 psia, throttled to a desired stagnation pressure, expanded through a contoured nozzle, and ejected to the atmosphere by vacuum pumps. Interchangeable throat sections were used to obtain test Mach numbers of 12.5 and 14.7.

Figure 2 shows the measured Mach number distribution within the test section as obtained from impact pressures on the tunnel center line and 1 inch above the center line. The solid line represents the predicted center line Mach number distribution for the Mach 14.7 nozzle.

A Mach number gradient of 0.33 per test-section diameter was measured with the Mach number 14.7 nozzle, and a Mach number gradient of 0.17 per test-section diameter was measured with the Mach number 12.5 nozzle. Although no extensive series of tests was performed to determine the exact edge of the boundary layer in the test section, a number of impact pressure surveys indicated that a 2-inch-diameter test core existed at the model location.

Instrumentation

A combination pressure transducer and teleducer system was used for measuring all pressures. Absolute pressures were measured with bonded strain gage differential pressure cells referenced to vacuum. Cells with maximum ranges of 1 and 15 psia, respectively, were used to obtain static and impact pressures. The transducers were subject to possible errors of ±0.10 percent of the full-scale reading. The over-all estimated error of the combination transducer-teleducer system was 0.002 psia.

Surface temperatures were obtained by measurement of the electromotive force output from thermocouples installed in the test body. The time rate of change of surface temperature was obtained by electrically amplifying and differentiating the emf output of the thermocouples. The temperature and time rate of change of temperature at each station was simultaneously recorded by two multichannel recording oscillographs.

A light-tight spark shadowgraph system was mounted on the tunnel side wall to allow visual interpretation of the flow. Shadowgraphs were obtained through flat window inserts of optical glass. A spark source located approximately 18 inches from the test body provided a point source of light for film exposure.

Test Body

Local pressure distribution and heat transfer were measured on the test body shown in figure 3. The leading edge was changed from sharp to blunt by attaching inserts with cylindrical leading edges to the lower surface of the 20° wedge. The leading-edge diameters were 1/32, 1/16, and 1/8 inch. Separate upper surface plates were used for the pressure distribution and heat-transfer tests.

A stainless-steel plate was screwed to the test body frame for the pressure distribution tests. Orifices, 0.040 inch in diameter, were spaced as shown in figure 3 and stainless-steel tubing with a 0.100-inch inside diameter transmitted the pressures to the tunnel exterior. The pressure tubes were connected to the transducers by 2-foot lengths of 1/8-inch-diameter neoprene tubing.

Heat-transfer measurements were made on a 0.029-inch-thick stainless-steel plate bonded to the test body frame with adhesive. Number 40 gage chromel-constantan thermocouple wires were spot-welded to the underside of the plate in the positions shown. These thermocouple wires went through the sting and model support to the tunnel exterior and were connected to a cold junction where they were changed to copper wire. From this junction, direct connections to the equipment for measuring temperature and temperature rate were made.

TEST METHOD

Before each test the stagnation chamber was subjected to a pressure somewhat higher than the desired stagnation pressure, and by means of a quick opening plug-type valve in the entrance to the nozzle throat, supersonic flow could be quickly established. Stagnation pressures were manually adjusted to 1300 and 1100 psia, respectively, for Mach numbers 14.7 and 12.5. Steady flow was established in less than 2 seconds. The test-section Mach number was verified by means of an impact probe located slightly ahead of and below the test body.

The model was positioned with its leading edge approximately 5 inches from the nozzle exit. Only data for the sharp and 1/32-inch leading edges are presented at Mach number 14.7 because established flow could not be attained for thicker leading edges. Alternate axial model positions did not alleviate this difficulty.

The run duration for the pressure measurements was governed by the time lag associated with the over-all pressure-recording system. The data-recording equipment was allowed to record repeatedly each transducer output until no further changes occurred. Then one final recording was made.

Previous to each heat-transfer test a tube with several cooling nozzles was inserted in the test section ahead of the model and liquid nitrogen was sprayed over the model to cool it to a desired temperature. The cooling tube was removed and tunnel flow was started. Temperatures and time rates of change of temperatures were recorded for 10 seconds before and after the tunnel started. The heat-transfer data presented herein were measured 2 seconds after the starting procedure was initiated. At this time the records indicated that near-isothermal conditions existed on the plate so that conduction and nonisothermal temperature corrections were negligible. When a theoretical heat balance was applied on an elemental volume of the plate surface and conduction and radiation terms were neglected, the local measured heat-transfer coefficient was given by

$$h = \frac{C \dfrac{dT_w}{d\theta}}{T_r - T_w} \tag{1}$$

For the present tests the recovery temperature was assumed to be given by

$$T_r = T\left[1+\sqrt{Pr}\left(\frac{\gamma-1}{2}\right)M^2\right] \tag{2}$$

Free-stream quantities were used in the right-hand side of equation (2) for the tests of the sharp plate and quantities were assumed for the local edge of the boundary layer for the tests of the blunt leading edge. The over-all estimated error of the measured heat-transfer coefficients was ±8 percent.

Shadowgraphs were taken of the flat plate with the 1/32-, 1/16-, and 1/8-inch-diameter leading edges at Mach number 12.5. Measurements of the shock-wave shapes were made with an optical comparator with a 10-to-1 magnification.

RESULTS AND DISCUSSION

Pressure Distribution

At the present time most of the helium tunnels are small in size and experimental measurements obtained in different facilities do not always agree. Tunnel size is probably one reason for such disagreement and therefore it is necessary to determine what effect it has on the present data. The measured ratios of surface static pressure to free-stream static pressure versus the distance from the leading edge of the flat plate are plotted in figures 4 and 5. Data were obtained with various leading-edge diameters and at Mach numbers 12.5 and 14.7. The empty-tunnel value of free-stream static pressure at each station was used to evaluate the pressure ratios. Included in figures 4 and 5 are the data measured downstream of the leading edge where the rate of change of pressure ratio with distance was no longer negative. This occurred at about 2.75 inches from the leading edge at Mach number 12.5 and about 2.25 inches at Mach number 14.7. The data aft of these distances should be disregarded since they are considered to be influenced by leading-edge shock-wave reflections from the effective tunnel wall and by Mach waves from the corners of the model leading edge. The data between the leading edge and the location where the pressure reversal occurs were not considered to be seriously influenced by span width. In reference 3 pressures measured on plates of different widths about one span back from the leading edge showed that no span effects were present. The ratio of model width to test core diameter was approximately the same for the present tests and those of reference 3 so span effects would probably not manifest themselves in the present data until at least a distance of one span width from the leading edge. Span effects would first be manifested off the model center line so pressures were measured during the present tests at orifices located 1.75 inches (1 span) and 2.75 inches (1.6 spans) from the leading edge midway between the model center line and the model side (see fig. 3). The deviation of the outboard pressures from the center line pressures was usually about -5 percent with a maximum of about -7 percent occurring on the 1/8-inch-diameter plate. The error in the data at these pressure levels was about ±5 percent and hence it was concluded that no serious span effects were present in the data.

Before the surface pressures on flat plates are examined in detail, it is desirable to establish the important variables and a theoretical background. As shown in figures 4 and 5 the pressure ratios at a given Mach number increase nonlinearly with increasing leading-edge diameter, and over the forward portion of the plate, decrease nonlinearly with increasing distance from the leading edge. Comparison of the tests at the two Mach numbers shows that the pressure ratios also increase with Mach number. In light of results from similar tests on plates at hypersonic Mach numbers, the 13-percent change in free-stream Reynolds number with test Mach number is considered to have a negligible effect on measured pressure ratio. Thus, over the present test range the important variables associated with the surface pressures were leading-edge thickness, distance from the leading edge, and free-stream Mach number.

Hypersonic flow over thin planar bodies, and, in particular, surface pressure prediction, was treated by Lees in reference 5. In this reference a wedge flow model was assumed for a flat plate with an attached shock wave at a Reynolds number, based on leading-edge thickness, of a few hundred. The wedge angle, η, with respect to the free-stream flow direction was assumed to represent the boundary-layer growth. Available hypersonic approximations for planar bodies along with the Prandtl boundary-layer equations were applied to this flow model. Two distinct flow regimes were discussed, the strong-interaction region where $M_\infty \eta \gg 1$ and the weak-interaction region where $M_\infty \eta \ll 1$. In either region the common term used in pressure prediction was the viscous interaction parameter.

To assess the general level and general trends shown by the data with the expected theoretical trends, the present data for the sharp plate will be compared with the theory of reference 5. The variation of the measured pressures for the sharp plate with the viscous interaction parameter is shown in figure 6. The solid line represents the first-order weak-interaction theory which for helium is

$$\frac{p}{p_\infty} = 1 + 0.62\chi_\infty \qquad (3)$$

Over the test range, equation (3) agrees reasonably well with the data. Based on available measuring techniques, the sharp leading-edged thickness could only be estimated as having a value between 0.001 and 0.00075 inch, giving leading-edge Reynolds numbers somewhere between 950 and 600. With such magnitudes of leading-edge Reynolds number, the criteria for the weak-interaction theory can be expected to prevail, provided the measurements are outside the region of leading-edge effects. The present data show this to be the case on these plates at distances greater than 750 leading-edge thicknesses. From the favorable comparison between the experimental results and the theoretically predicted trends for a sharp leading-edge plate there appear to be no gross experimental errors present and attention will now be directed to the problem of the flow over blunt plates.

The complexity of the problems encountered in the prediction of the flow field over flat plates with leading-edge bluntness sufficient to cause measurable shock-wave detachment makes purely theoretical approaches difficult, except in the limiting case of a very thick leading edge. For this reason most of the work involving blunt plates at very high Mach numbers is experimental and correlation of surface pressures is usually semiempirical (see refs. 3, 4, and 6). For the present tests such a correlation which includes all the important variables associated with surface pressures is not practical because of the limited Mach number range and the limited test data at Mach number 14.7. However, because of the wide range of leading-edge thickness tested at Mach number 12.5, an attempt will be made to show the effect of this variable on measured surface pressure.

In the limit as the leading edge becomes very thick, viscous effects are no longer present and surface pressures should correlate on inviscid parameters. The plane blast wave theory (see ref. 7) as applied to the problem of hypersonic flow over a flat plate provides such parameters. Two important results derived from the theory are

$$\frac{R}{d} = K_1 \left(C_{D_N}\right)^{1/3} \left(\frac{x}{d}\right)^{2/3} \tag{4}$$

$$\frac{\Delta p}{p_\infty} = K \left(\frac{C_{D_N}}{x/d}\right)^{2/3} M_\infty^2 \tag{5}$$

Equation (4) relates the shock-wave shape to the distance along a planar body. Equation (5) relates the pressure rise above the undisturbed pressure to the energy associated with the nose drag, the distance along the planar body, and the flight Mach number. Blast-wave theory would predict for a fixed Mach number and leading-edge shape that pressures correlate with x/d. Figure 7(a) shows this not to be the case for the present data. Other investigators have found that data for blunt plates did not correlate with x/d (e.g., refs. 3, 4, 8) and they have introduced a leading-edge Reynolds number term to obtain correlation. For the present data a 1/4 power of Re_d provides correlation as shown in figure 7(b). This use of Re_d has the limitation that the correlation must break down as $Re_d \to \infty$; however, it suggests that the systematic differences found are due to viscous effects. Additional tests, particularly at large Re_d are needed to determine whether this inference is correct.

Shadowgraph Observations

The shape of the shock waves over blunt plates is of interest for (1) comparing with predicted shock-wave shapes, (2) predicting the radiation heat transfer over blunt leading edges, and (3) estimating the

vorticity introduced into the flow fields over blunt wings. For these reasons the shock-wave shapes obtained during the current investigation are presented. Two methods were used to correlate the shock-wave shapes. The first consisted in using the basic assumptions provided by Moeckel in reference 9 that the shock wave was hyperbolic, normal to the free-stream direction on the axis of symmetry, and asymptotic to the free-stream Mach line at a great distance from the axis of symmetry. The second method was to apply the blast-wave analogy which relates the shock-wave shape to the energy imparted to the wave by the pressure drag of the leading edge.

Figure 8 shows the shadowgraph pictures of the blunt plates at Mach number 12.5. Measured shock-wave shapes over the surface of the blunt plates at zero angle of attack are shown in figure 9. In this figure R is the perpendicular distance to the outer edge of the shock wave above the plate measured from a plane parallel to the free stream and passing through the vertex of the shock wave. The term $(x+\Delta)$ is the distance along a plane parallel to the upper surface of the plate measured from the vertex of the shock wave. Both distances were normalized with respect to the leading-edge diameter. The spread of the data noted in figure 9 might be due to nonparallel light rays which were inherent in the use of the shadowgraph. The solid line was obtained by a modification of Moeckel's approximate method for calculating the shock-wave shape. In order to match the predicted and measured shock-wave locations, an adjusted asymptote was used rather than the value given by the cotangent of the free-stream Mach line. A similar modification was used in reference 10 to predict shock-wave shapes over blunt plates in air at Mach numbers up to 4.7. The general shape of the curve is given by

$$\frac{R}{d} = \beta_o^{-1}\left[\left(\frac{x+\Delta}{d}\right)^2 + 2\,\frac{x_o}{d}\left(\frac{x+\Delta}{d}\right)\right]^{1/2} \tag{6}$$

Numerical values for β_o and x_o/d were obtained by a trial and error fitting of equation (6) to the measured data and were found to be 4.0 and 23, respectively. Reference 10 postulated that the value of β_o was a function of test conditions and leading-edge configuration, but no specific variations were indicated. No conclusions about the dependence of β_o on these variables can be made for the present tests. Generally, the position of the curve is matched well by equation (6) but the local slopes differ from those of the data.

The dashed line in figure 9 represents the best straight-line fit to the data as obtained by the method of least squares. It can be expressed in equation form as

$$\frac{R}{d} = 1.64\left(\frac{x+\Delta}{d}\right)^{0.59} \tag{7}$$

Equation (7) is similar to the derived expression for shock-wave shape from the blast wave analogy given in equation (4). In equation (4) the constant of proportionality for helium is 0.975, and when combined with the nose drag coefficient to the 1/3 power yields the equation

$$\frac{R}{d} = 1.036 \left(\frac{x}{d}\right)^{0.66} \tag{8}$$

Except in the vicinity of the leading edge, the shock-wave detachment distance is negligible and comparison of equations (7) and (8) indicates that although the exponents of the dimensionless distance from the shock-wave vertex differ by 10 percent, the intercept values differ by 60 percent. The blast-wave analogy tends to give the correct curvature of the shock wave but fails to give the exact position of the wave. In reference 4 a similar result is reported.

A comparison of the two methods indicates that over the present range of leading-edge thickness, a similar expression to that of the plane blast-wave theory gives the better representation of the data for distances from 2 to 50 diameters behind the leading edge. Data for $\left(\frac{x+\Delta}{d}\right) < 1$ were omitted because nonparallel light and measuring inaccuracies in that vicinity caused a great deal of scatter in the data. However, there was a trend to those data which indicated that the shock-wave shape was hyperbolic near the leading edge.

Shock-wave shape was also measured over the undersurface of the model which was a blunt 20° wedge (see fig. 3). While this was the only wedge angle or angle of attack that was investigated, it is interesting to examine the effect of this variable on the shock-wave shape. Figure 10 shows the normalized shock-wave shape near the leading edge below the plane parallel to the free-stream and passing through the shock-wave vertex. The solid line gives the shock-wave shape obtained from oblique shock-wave relations for a two-dimensional sharp wedge. The origin of the sharp wedge was at the intersection of the planes of the upper surface of the flat plate and the lower surface of the wedge. Specifically the expression was

$$\frac{R}{d} = 1.4 + \tan\delta \left(\frac{x+\Delta}{d}\right) \tag{9}$$

where the numerical constant accounts for an origin shift and δ is the angle of inclination of the oblique shock wave with the free-stream direction. The results of figure 10 show that shock-wave shape over a blunt 20° wedge can be predicted by sharp-wedge theory.

Heat Transfer

One of the objectives of the present investigation was to compare the measured heat-transfer coefficients with those predicted from available solutions of the compressible laminar boundary-layer equations. However, since few measurements of heat transfer have been made on flat plates in helium at these high Mach numbers, it is of interest to examine the data for expected trends before comparing it with theory.

Local surface heat-transfer coefficients at the two test Mach numbers are presented in figures 11 and 12. The data points represent the average of five test runs in which the maximum scatter of the data was ±8 percent. The ratio of wall temperature to stagnation temperature was maintained between 0.65 and 0.75. A comparison of the data for the same leading-edge diameter at the two test Mach numbers, as shown in figures 11(b) and 12(b), shows a slight decrease in heat-transfer coefficient with increasing Mach number. This behavior is what would be expected from theoretical considerations. At a fixed position downstream of the leading edge, increasing the bluntness resulted in an increase in the heat-transfer coefficient. This increase was caused mainly by the higher surface pressures produced by the blunter leading edges. The increased heat transfer 2 inches behind the leading edge of the plate at a Mach number of 14.7 indicates that Mach waves from the corners of the leading edge and the effective tunnel wall were influencing the data. This same effect was evident in the surface pressure measurements as noted earlier That this increase could be caused by transition to turbulent flow is doubtful since the local Reynolds numbers at a Mach number of 12.5 are greater than at a Mach number of 14.7.

The predicted heat-transfer coefficients on the sharp plate for the two test Mach numbers are shown as the solid line curves in figures 11(a) and 12(a). They were calculated from

$$h = \left(-\frac{S_w'}{S_w}\right)\sqrt{\frac{\rho_\infty u_\infty \mu_\infty}{s}}\, C_{p_\infty} \sqrt{2(1+n)\,\frac{p}{p_\infty}} \qquad (10)$$

which was obtained from references 11 and 12. In the derivation of this equation the usual assumptions of a thin boundary layer, constant specific heat, and constant Prandtl number were made. However, additional assumptions regarding the effects of pressure gradient along the plate, variable viscosity, and compressibility were also taken into consideration. Although a particular type of pressure gradient variation along the plate was assumed in order to simplify the mathematics, Stine and Wanlass (ref. 13) show that for a small variation of pressure gradient, such as that measured along the sharp plate in the current study, the solution presented in reference 11 should be adequate to account for the effects of this variable.

The reasonably good agreement between the measured and calculated heat transfer indicates that there are no basic discrepancies in the data and that a theory which was developed for air but neglects real gas effects (i.e., changes in c_p, γ, and chemistry) is adequate to predict heat transfer in helium flows. Attention is now directed toward the data obtained on the plates with blunt leading edges.

When shock-wave detachment occurs at the blunt leading edge, equation (10) is no longer valid. Several methods for predicting heat transfer to blunt plates in air have proven successful at supersonic Mach numbers, provided the proper definition of the local conditions along the boundary-layer edge were made. See, for example, references 12, 13, and 14. In order to compare these methods with the present test results it was assumed that the total pressure at the edge of the boundary layer was constant and equal to the reduced total pressure behind a normal shock wave at the free-stream Mach number. Using measured surface pressures and assuming isentropic expansion along the boundary-layer edge together with the above assumptions provided sufficient information to define the local conditions.

The simplest method used to calculate heat-transfer coefficients was the well-known Pohlhausen solution for local heat transfer across a laminar boundary layer. In order to account for compressibility and Mach number effects, the local value of Reynolds number along the boundary-layer edge was used and the fluid properties were evaluated at the T* reference temperature from reference 15. Expressed in equation form

$$h = 0.332 \sqrt{Re^*_{se}}\, Pr^{*^{1/3}} \frac{k^*}{s} \qquad (11)$$

where the starred quantities signify local properties evaluated at the reference temperature. The more exact solutions given in references 11 and 13 were also considered but little difference in the final result was obtained (see fig. 11(d)). Therefore, equation (11) was used for comparison with the data. Agreement of equation (11) and the test data from the blunt plates was not obtained over the complete test range. At both Mach numbers a reasonable prediction was obtained for the 1/32-inch leading-edge data back to 1.5 inches from the leading edge but thereafter the measured heat transfer became higher than that of theory by more than 30 percent. For the other two leading edges the prediction was adequate only at the 1/2-inch station. In general, theory gave low values of h and the deviation from the data became greater with increasing leading-edge bluntness.

Several possible reasons for the discrepancy between data and theory may be offered: none of the methods account for the true history of the boundary layer ahead of the points in question; the assumption of constant total pressure at the edge of the boundary layer may not be valid or the value assumed for the total pressure may be incorrect; above the plate in a direction normal to the plate surface the rate of change of velocity

is not zero at the boundary-layer edge as assumed in the theories used in the current study. The unfavorable comparison of theory and experiment clearly indicates that a more complete knowledge of the flow field over blunt plates is necessary before adequate predictions of convective heat transfer can be made.

CONCLUDING REMARKS

Surface pressures on plates with leading-edge Reynolds numbers between 600 and 950 were predicted by the hypersonic weak-interaction parameter at distances from the leading edge greater than 750 leading-edge thicknesses and showed that complete dissipation of leading-edge effects was accomplished. At a Mach number of 12.5 the measured pressures on blunt plates with leading-edge Reynolds numbers greater than 25,000 were found to vary as $Re_d^{-0.25}$.

Shock-wave shapes over blunt plates were found to agree with the blast-wave analogy in modified form at distance from 2 to 60 diameters aft of the shock-wave vertex.

Convective heat transfer on the surface of sharp flat plates at hypersonic Mach numbers with moderate axial pressure gradient can be predicted by existing exact solutions of the laminar boundary-layer equations. However, a more complete knowledge of the flow field between the shock wave and the body surface is necessary before an adequate prediction can be made of heat transfer to blunted plates at very high Mach numbers.

Ames Research Center
National Aeronautics and Space Administration
Moffett Field, Calif., Nov. 2, 1960

REFERENCES

1. Matting, Fred W., Chapman, Dean R., Nyholm, Jack R., and Thomas, Andrew G.: Turbulent Skin Friction at High Mach Numbers and Reynolds Numbers. Heat Transfer & Fluid Mechanics Inst., 1959. NASA OTP-1959.

2. Creager, Marcus O.: High Altitude Hypervelocity Flow Over Swept Blunt Glider Wings. IAS Paper No. 59-113, June 1959.

3. Henderson, Arthur, Jr., and Johnston, Patrick J.: Fluid Dynamic Properties of Some Simple Sharp and Blunt Nosed Shapes at Mach Numbers From 16 to 24 in Helium Flow. NASA MEMO 5-8-59L, 1959.

4. Vas, I. E., and Bogdonoff, S. M.: Hypersonic Studies of Blunt Unswept Wings. Princeton Univ., Dept. of Engineering, Rep. 450, April 1959.

5. Lees, Lester: Hypersonic Flow. GALCIT Pub. No. 404, 1955.

6. Bertram, Mitchell H., and Baradell, D. L.: A Note on the Sonic-Wedge Leading-Edge Approximation in Hypersonic Flow. Jour. Aero. Sci., vol. 24, no. 8, Aug. 1957, pp. 627, 628.

7. Rogers, M. H.: Similarity Flows Behind Strong Shock Waves. Quart. Jour. Mech. and Appl. Math., vol. XI, pt. 4, Nov. 1958, pp. 411-422.

8. Vas, Irwin E.: An Experimental Investigation of the Pressure on a Thin Flat Plate at Hypersonic Speeds. Princeton Univ., Dept. of Engineering, Rep. 377, March 1957.

9. Moeckel, W. E.: Approximate Method for Predicting Form and Location of Detached Shock Waves Ahead of Plane or Axially Symmetric Bodies. NACA TN 1921, 1949.

10. Tendeland, Thorval, Nielson, Helmer L., and Fohrman, Melvin J.: The Flow Field Over Blunted Flat Plates and Its Effect on Turbulent Boundary-Layer Growth and Heat Transfer at M = 4.7. NASA TN D-689, 1961.

11. Cohen, Clarence B., and Reshotko, Eli: Similar Solutions for the Compressible Laminar Boundary Layer with Heat Transfer and Pressure Gradient. NACA Rep. 1293, 1956.

12. Bertram, Mitchell H., and Feller, William V.: A Simple Method for Determining Heat Transfer, Skin Friction, and Boundary-Layer Thickness for Hypersonic Laminar Boundary-Layer Flows in a Pressure Gradient. NASA MEMO 5-24-59L, 1959.

13. Stine, Howard A., and Wanlass, Kent: Theoretical and Experimental Investigation of Aerodynamic-Heating and Isothermal Heat-Transfer Parameters on a Hemispherical Nose With Laminar Boundary Layer at Supersonic Mach Numbers. NACA TN 3344, 1954.

14. Creager, Marcus O.: Effects of Leading-Edge Blunting on the Local Heat Transfer and Pressure Distributions Over Flat Plates in Supersonic Flow. NASA TN 4142, 1957.

15. Rubesin, M. W., and Johnson H. A.: A Summary of Skin Friction and Heat Transfer Solutions of the Laminar Boundary Layer of a Flat Plate. Amer. Soc. of Mech. Engrs., Trans. vol. 71, no. 4, May 1949, pp. 383-388.

16. Mueller, James N.: Equations, Tables, and Figures for Use in the Analysis of Helium Flow at Supersonic and Hypersonic Speeds. NACA TN 4063, 1957.

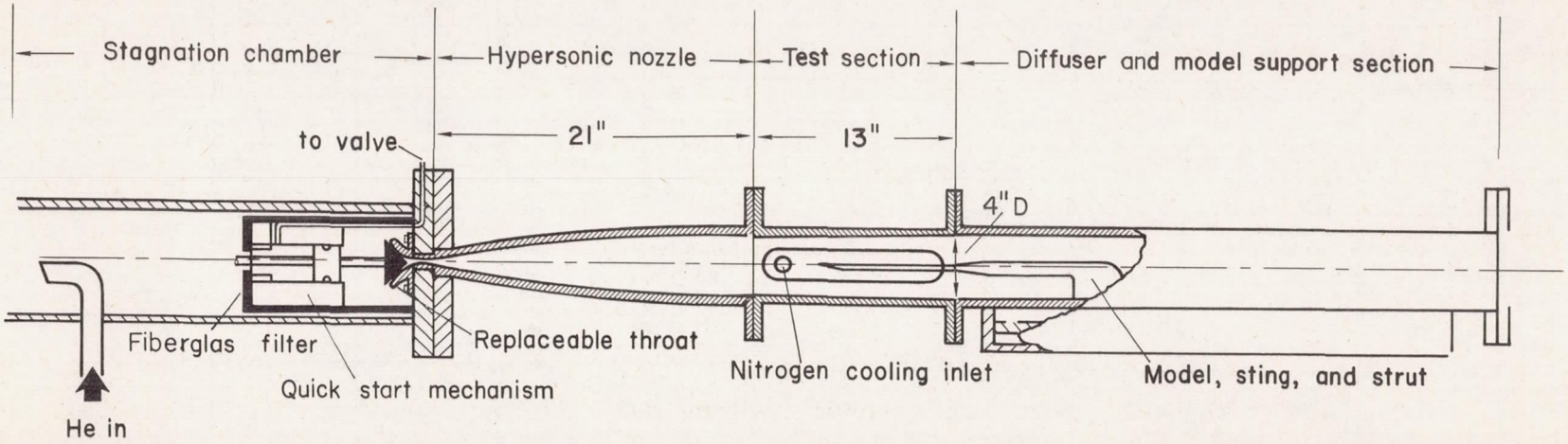

Figure 1.- Schematic diagram of 4-inch-diameter pilot helium wind tunnel.

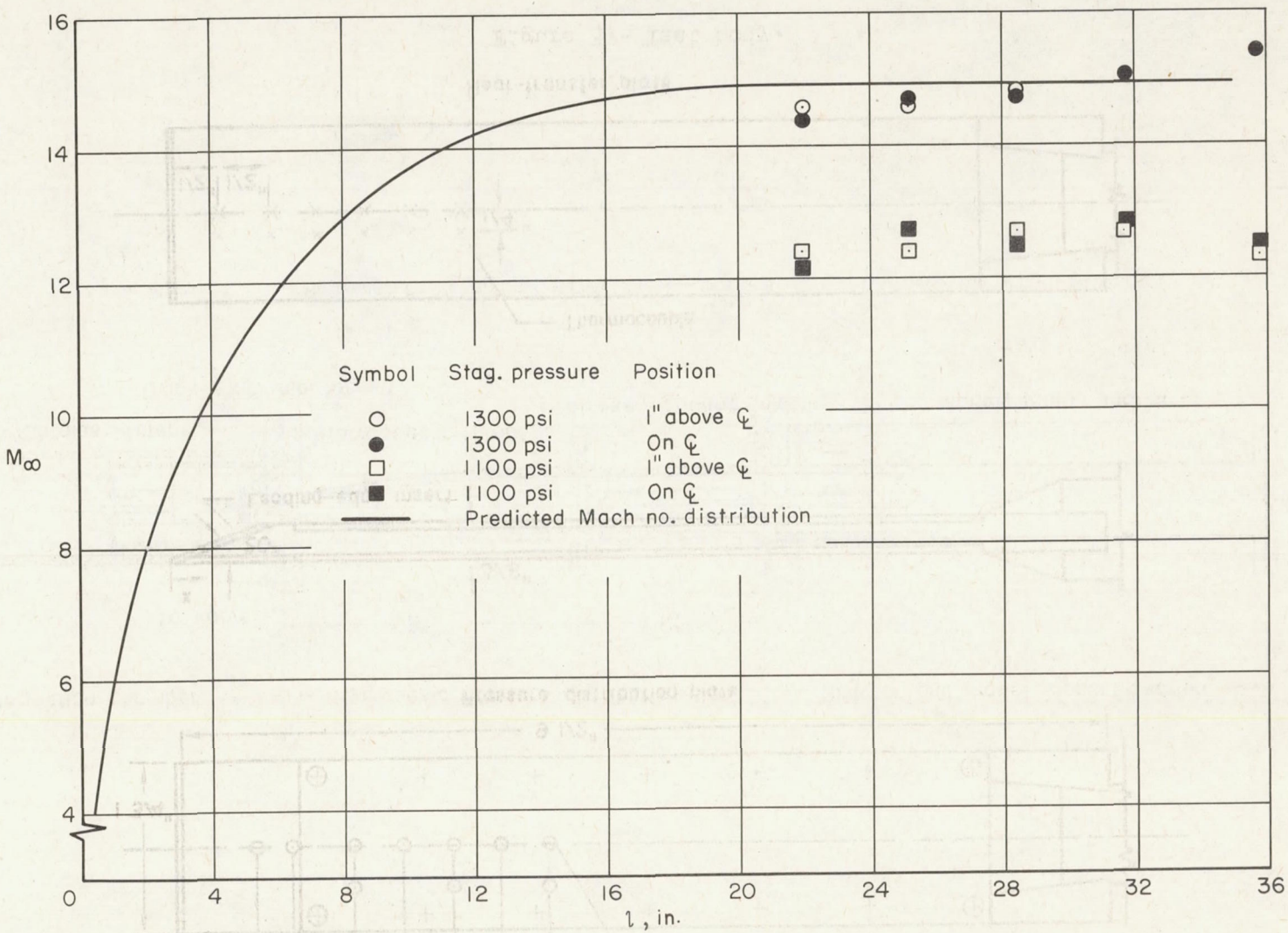

Figure 2.- Tunnel Mach number distribution for two throat inserts.

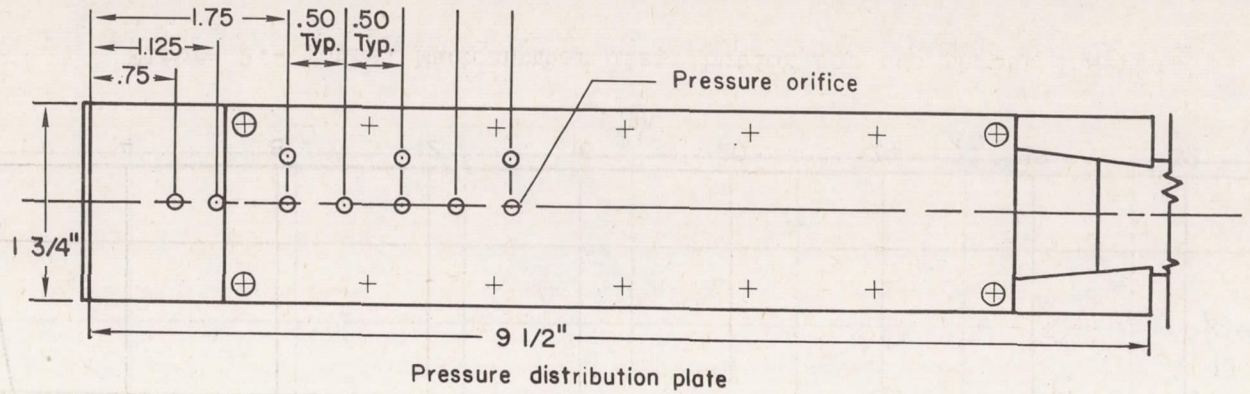

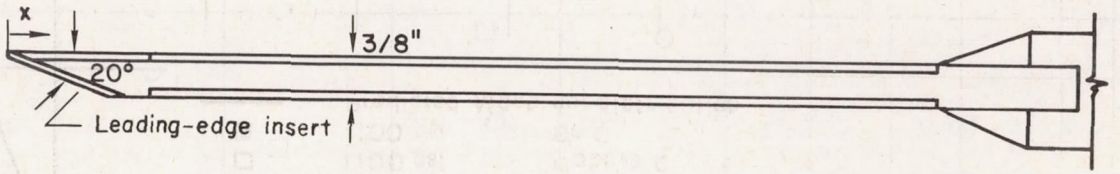

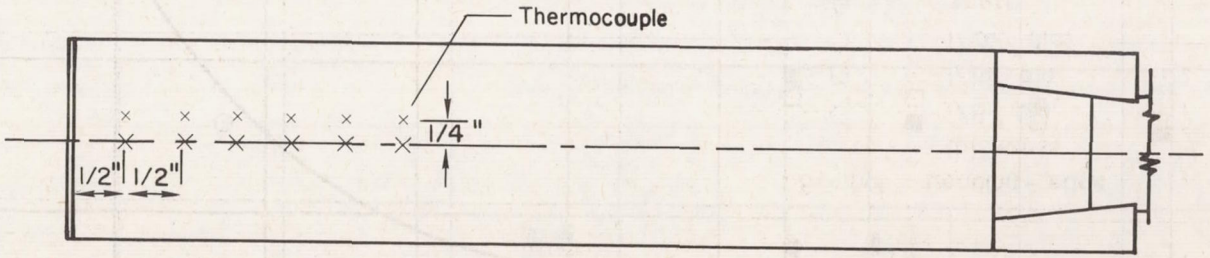

Figure 3.- Test body.

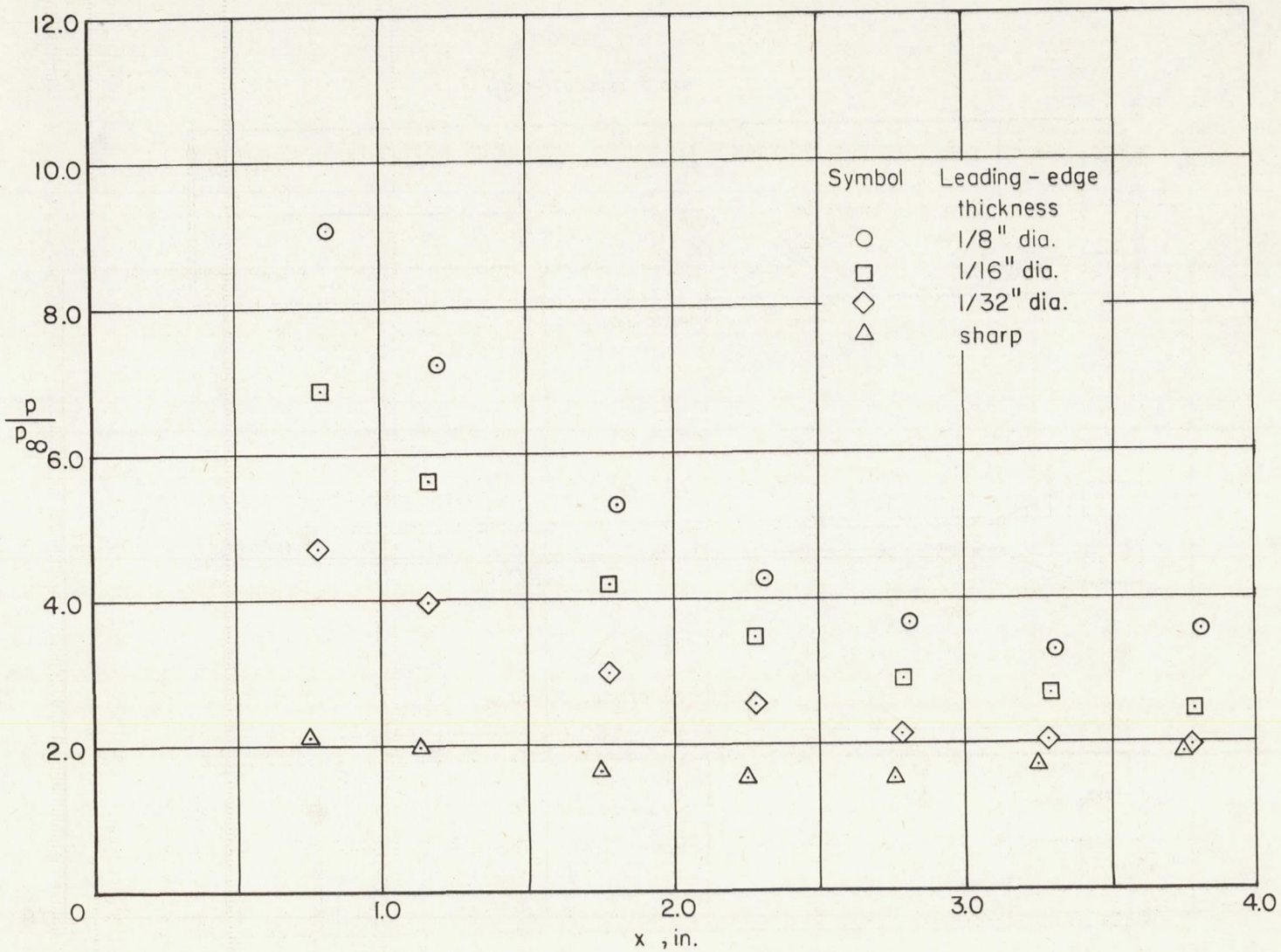

Figure 4.- Measured pressure ratio on unswept blunted plates at $M_\infty = 12.5$.

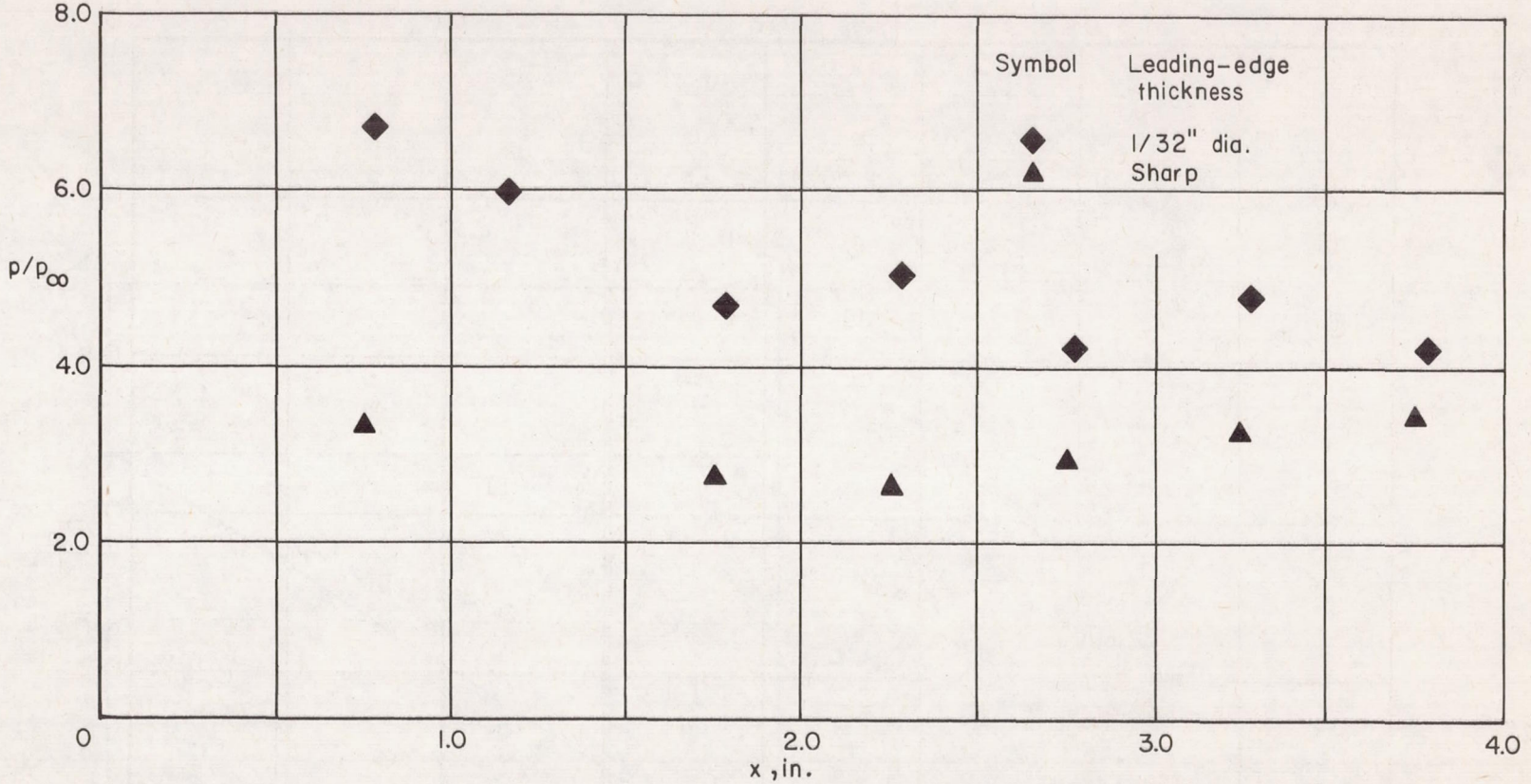

Figure 5.- Measured pressure ratio on unswept blunted plates at $M_\infty = 14.7$.

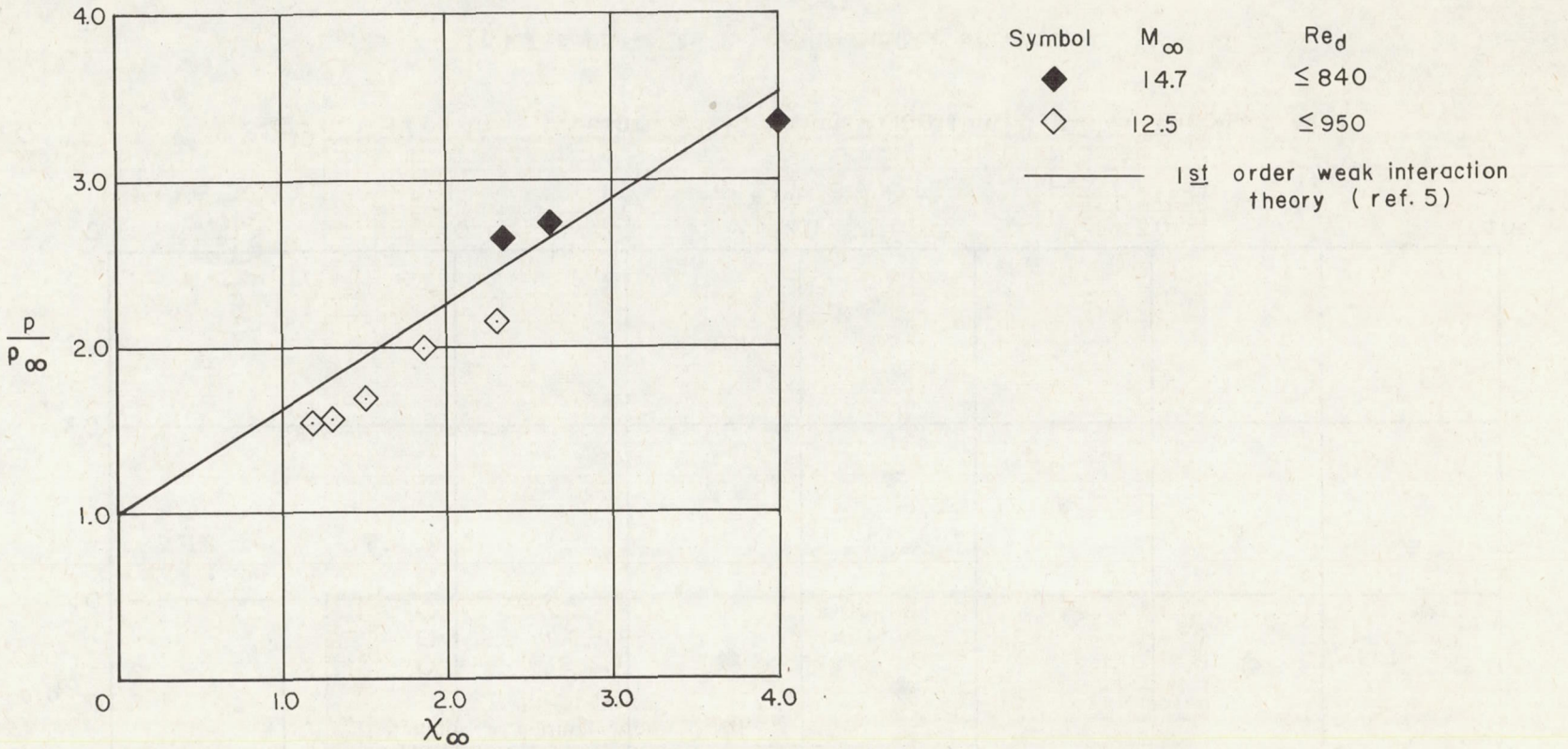

Figure 6.- Variation of measured pressure ratio on a sharp flat plate with the viscous interaction parameter.

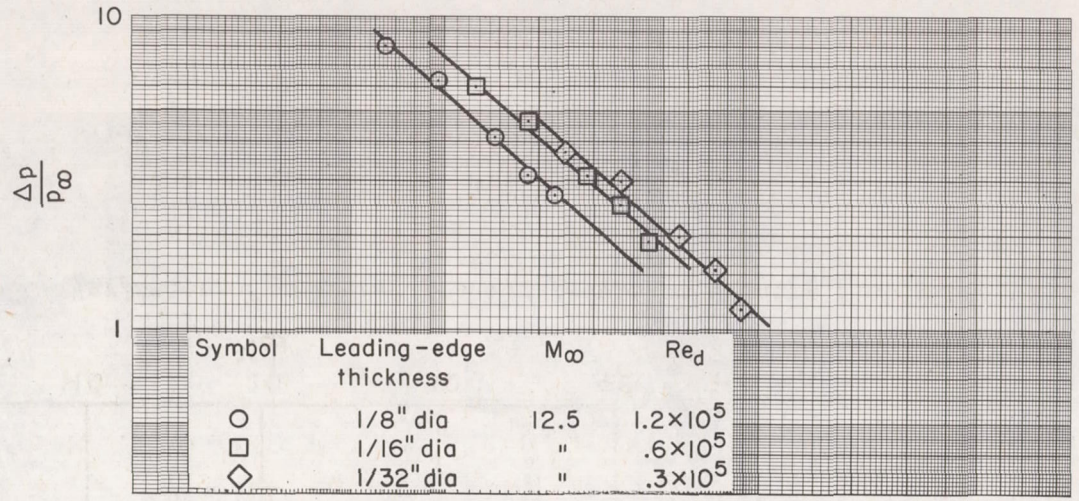

(a) Measured surface pressures.

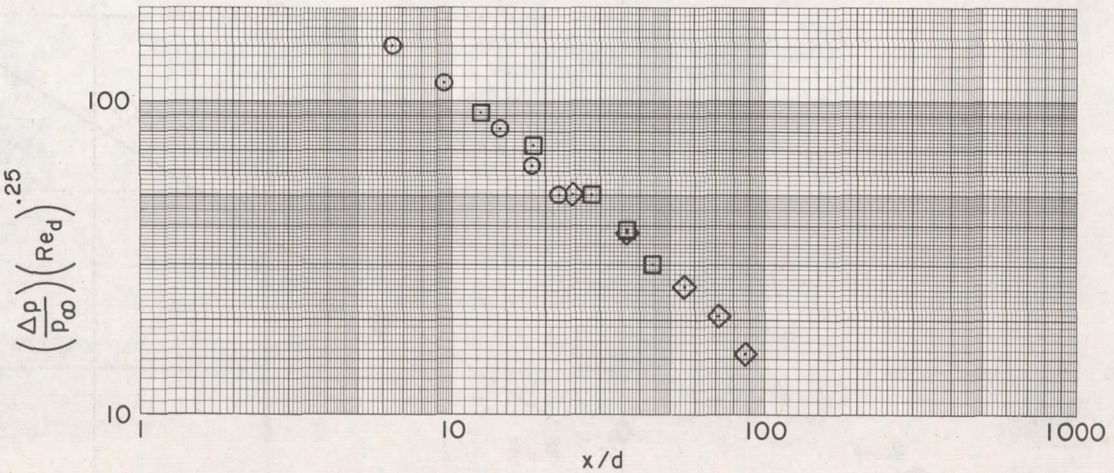

(b) Leading-edge Reynolds number effect.

Figure 7.- Correlation of surface pressures at $M_\infty = 12.5$.

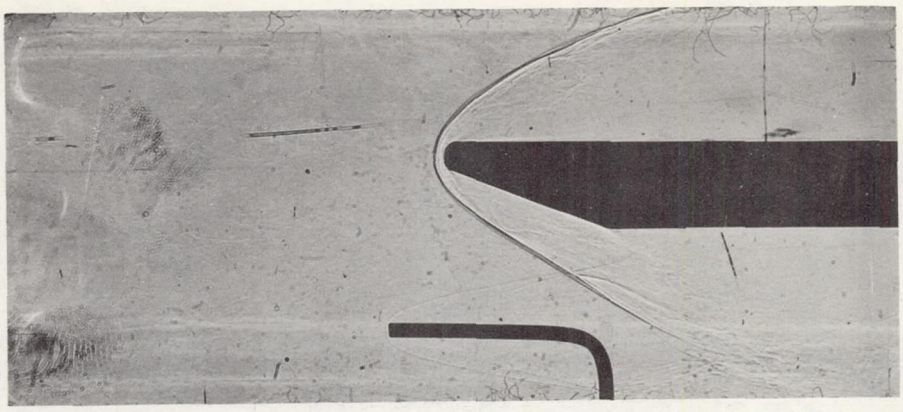

(a) 1/8-inch-diameter leading edge.

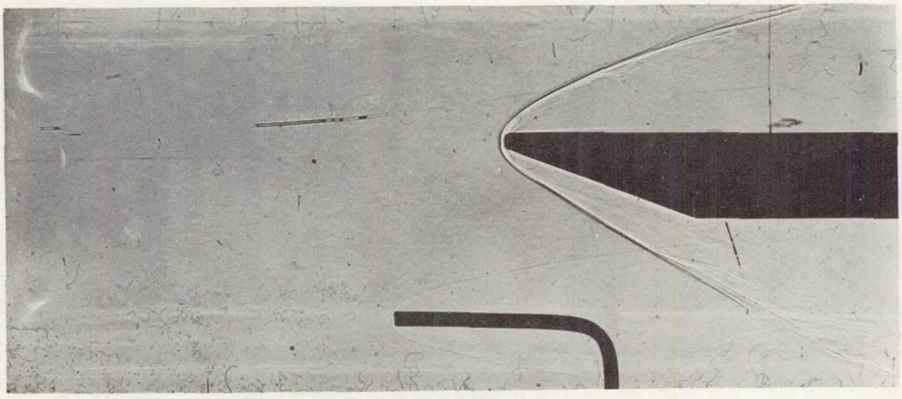

(b) 1/16-inch-diameter leading edge.

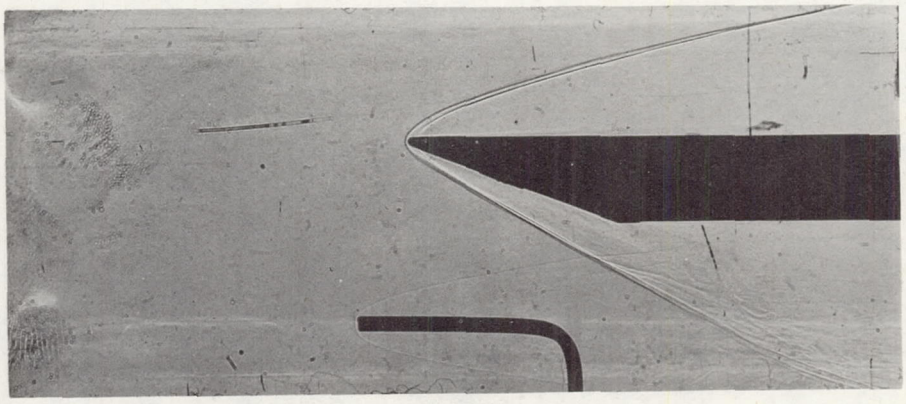

(c) 1/32-inch-diameter leading edge.

Figure 8.- Shadowgraphs of blunt leading-edged plates at $M_\infty = 12.5$.

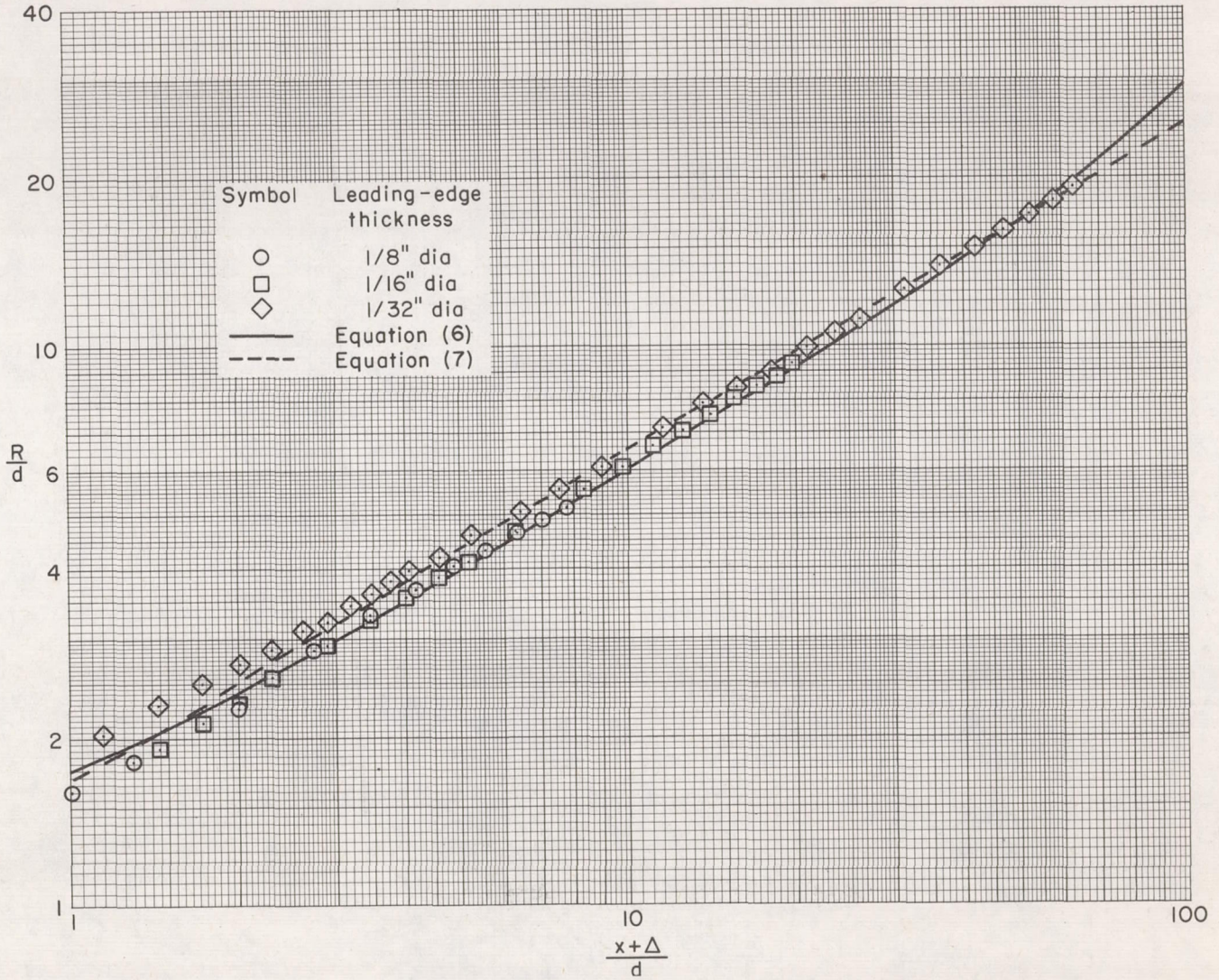

Figure 9.- Measured shock-wave shapes over blunted plates at $M_\infty = 12.5$.

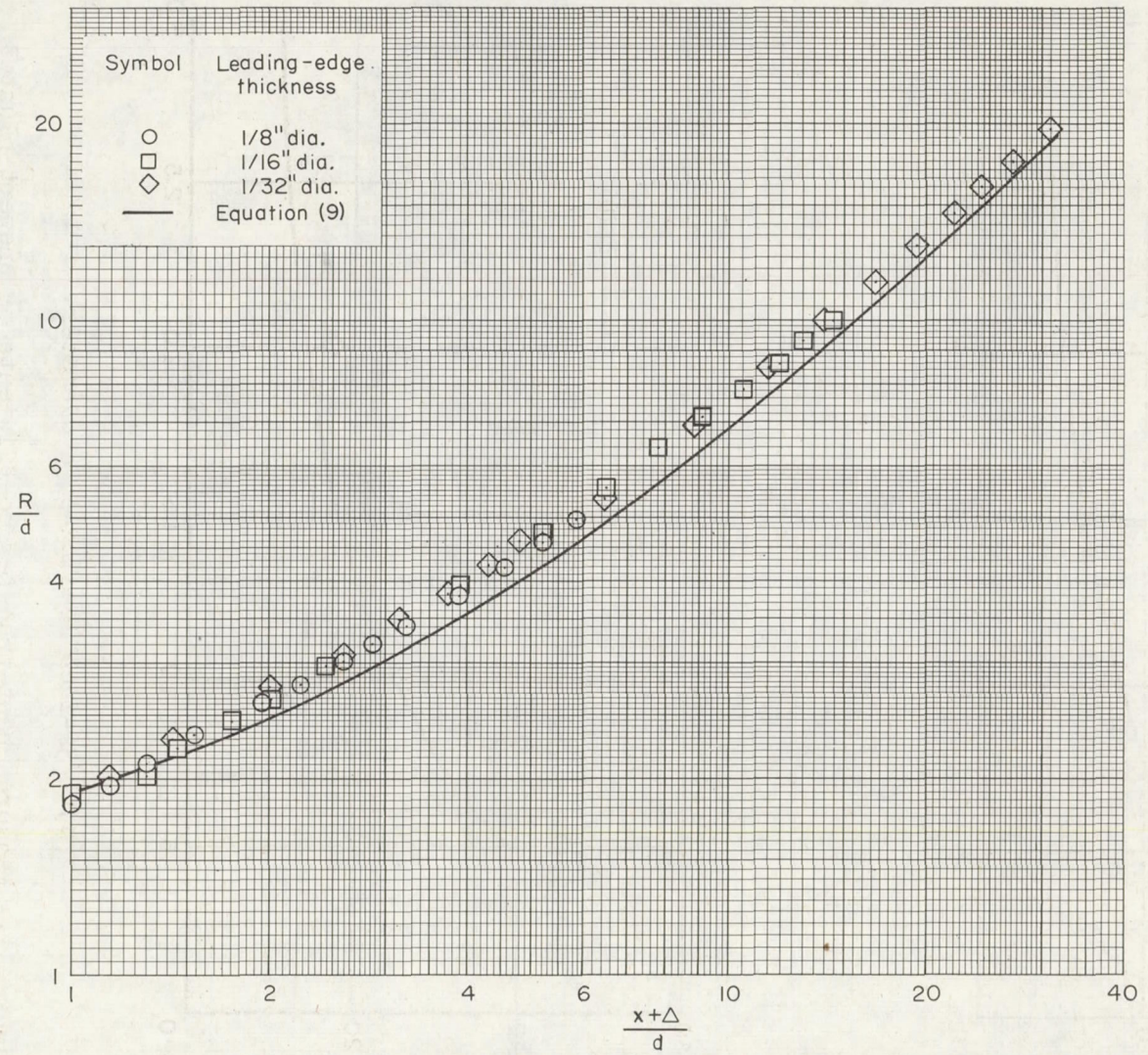

Figure 10.- Measured shock-wave shape over blunted 20° wedge portion of the model leading edge at $M_\infty = 12.5$.

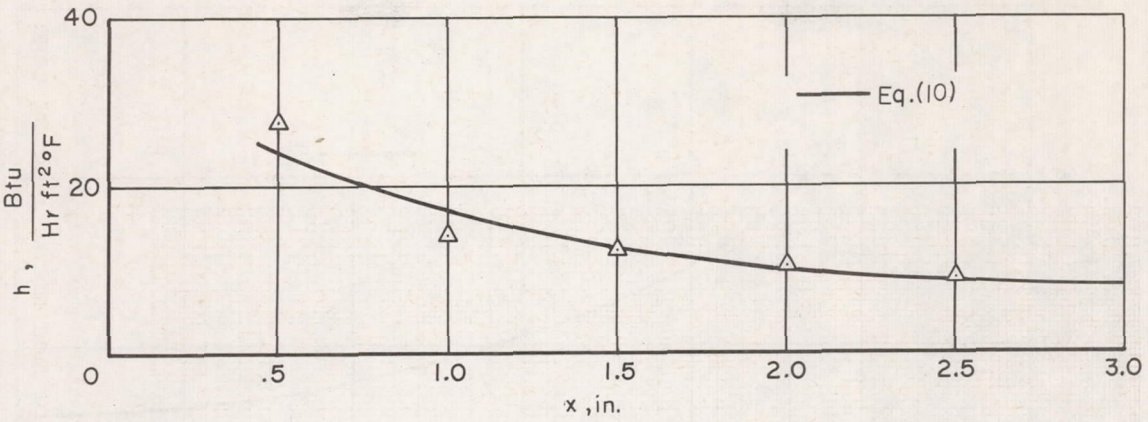

(a) Sharp leading edge.

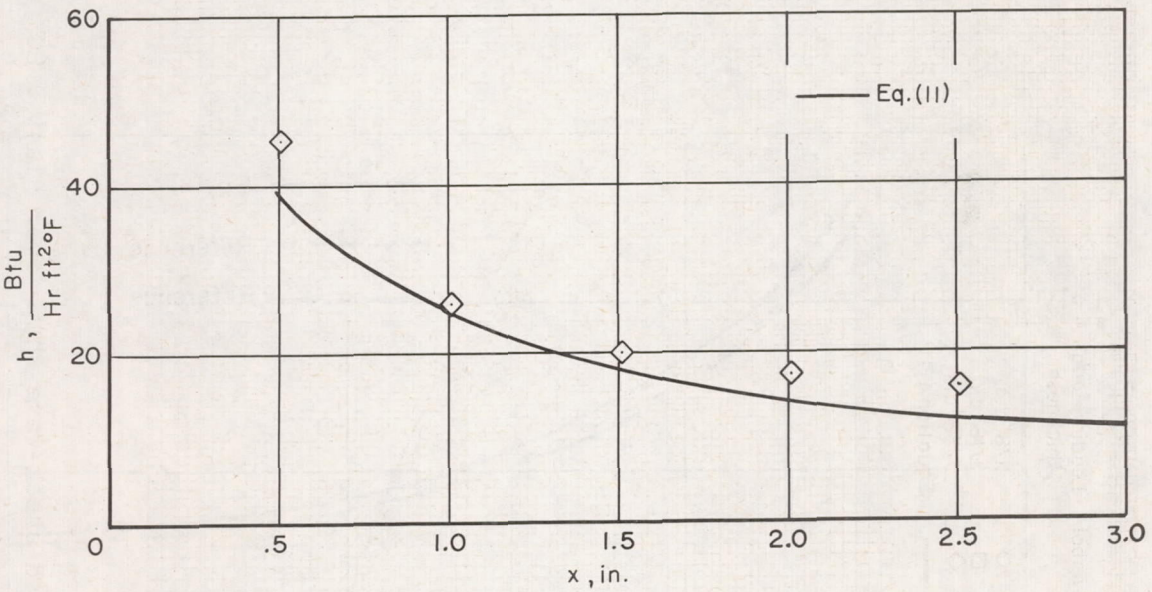

(b) 1/32-inch leading-edge diameter.

Figure 11.- Measured heat-transfer coefficients on unswept blunted plates at $M_\infty = 12.5$.

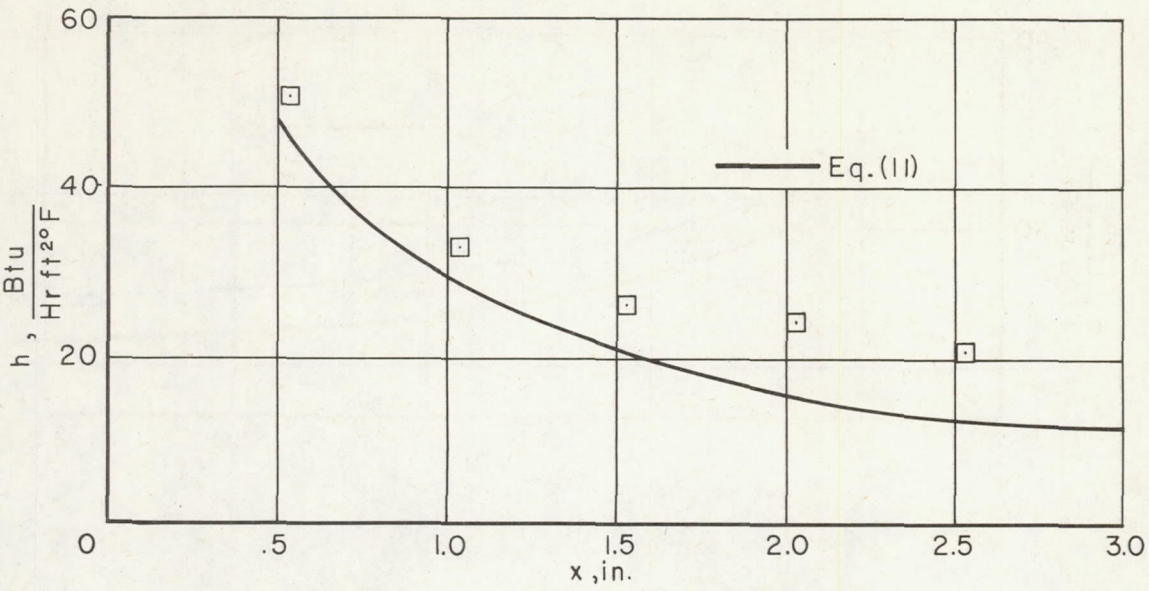

(c) 1/16-inch leading-edge diameter.

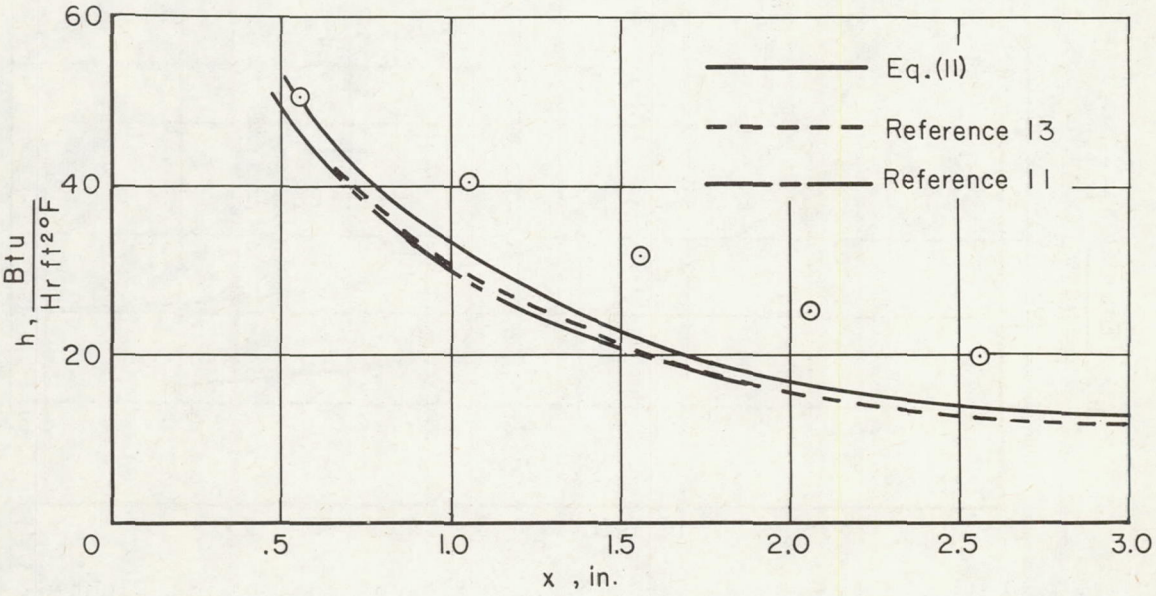

(d) 1/8-inch leading-edge diameter.

Figure 11.- Concluded.

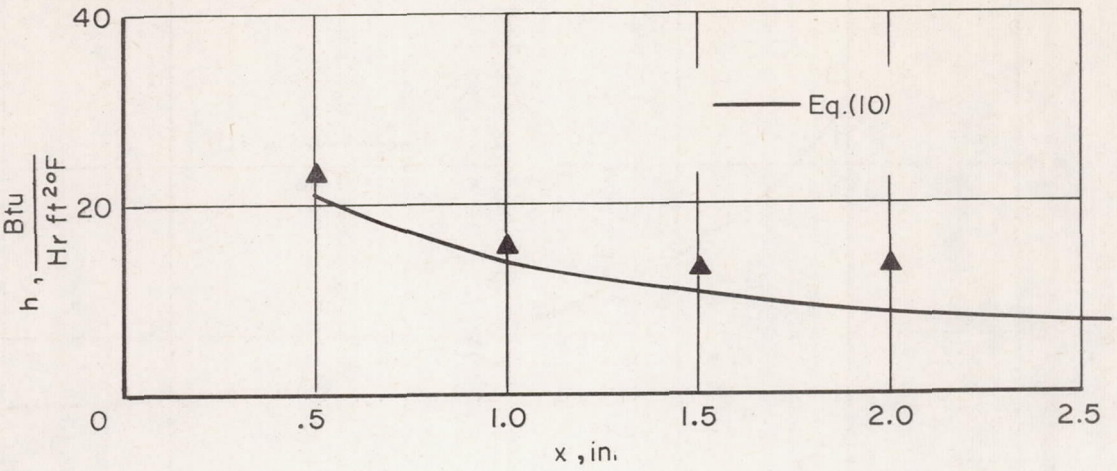

(a) Sharp leading edge.

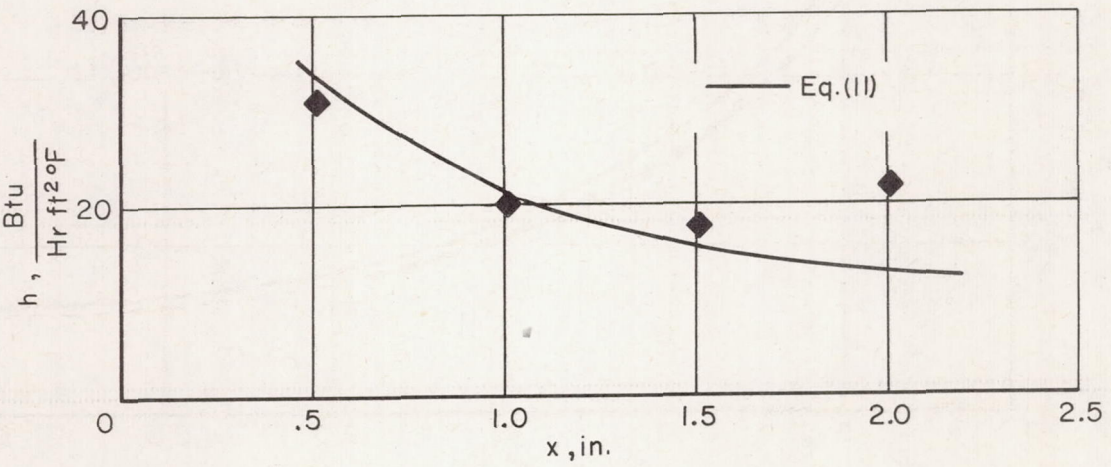

(b) 1/32-inch leading-edge diameter.

Figure 12.- Measured heat-transfer coefficients on unswept blunted plates at $M_\infty = 14.7$.